International Journal of Control, Automation and Systems 19(11) (2021) 3698-3707
http://dx.doi.org/10.1007/s12555-020-0913-8
ISSN:1598-6446 eISSN:2005-4092
http://www.springer.com/12555

Control of a Non-uniform Flexible Beam: Identification of First Two Modes

Phuong-Tung Pham, Gyoung-Hahn Kim, Quoc Chi Nguyen*, and Keum-Shik Hong

Abstract: This paper presents an experimental study implementing the input shaping control of the first two modes of the vibration of a non-uniform flexible cantilever beam having a translating base. Examples of a moving cantilever beam appear in many industrial systems. Vibration suppression of the beam has important implications for improving the effectiveness of such systems. The equations of motion of the cantilever beam, including the moving base, are developed using the extended Hamilton principle. The partial differential equation representing the beam's dynamics is then transformed into a finite-dimensional model using the Galerkin method. Accordingly, the modal parameter identification procedure is established based on experimental modal analysis. Under the estimated modal parameters, including the natural frequency and damping ratio, single- and two-mode input shaping controllers of three different types (zero vibration, zero vibration derivative, and zero vibration derivative-derivative) are designed for vibration suppression of the beam. Experimental results are discussed, reporting that the two-mode shaper's vibration suppression was superior to the single-mode shaper. In contrast, the two-mode shaper's settling time has slightly increased compared to that of the single-mode shaper.

Keywords: Experimental modal analysis, flexible beam, input shaping control, modal parameter identification, non-uniform beam, vibration suppression.

1. INTRODUCTION

The cantilever is a ubiquitous structure applied in various fields, including civil engineering, aerospace, and mechanical engineering. Typical cantilever applications include a cantilever bridge, aircraft wings, master fuel assembly in nuclear refueling machines, electromechanical monolithic resonator in micro-electromechanical systems, drills, and microinjection robots; see Fig. 1. A cantilever can be modeled rigid or flexible depending on its flexibility. In heavy-weight systems with slow dynamics, the cantilever is a rigid structure, and its vibration can be ignored due to the high material stiffness. In contrast, a flexible cantilever's vibration in light-weight systems can significantly affect the system's performance and safety. Such vibration problem is aggravated when the flexible cantilever moves at high speed. Therefore, analysis and suppression of the vibration of flexible cantilevers are desired.

From an engineering perspective, beam models can be used to describe cantilevers. The beam model considers the bending stiffness of the material (i.e., Euler–Bernoulli beam [2–4]) and further examines the shear deformation and cross-sectional rotation (i.e., Timoshenko beam [5–7]). A flexible cantilever beam is a distributed parameter system with an infinite number of vibration modes [8]. Partial differential equations (PDEs) governing the flexible beams' dynamics have been developed based on the extended Hamilton principle [9–11]. Early studies on flexible cantilever beams focused on stationary beams' dynamics, where one end of the beam is clamped into a fixed base, and the other end is free [12,13]. Besides stationary beams, moving beams with a translating or rotating base (referred to as translating [2,14] and rotating [9,15,16] beams, respectively) have also been investigated. In this case, the vibration of the beam is a direct result of the base's motion. Therefore, the dynamics of a moving base and its connected beam have been investigated [15,17,18]. A flexible system's dynamic behaviors are characterized by the modal parameters, including the natural frequency, damping ratio, and mode shape. Analysis of these parameters is often performed based on a finite-dimensional model [19,20]. The finite-dimensional

Manuscript received December 9, 2020; revised February 4, 2021; accepted February 21, 2021. Recommended by Editor Kyoung Kwan Ahn. This research was funded in part by Vietnam National University Ho Chi Minh City (VNU-HCM) under grant no. C2018-20-01 and in part by the National Research Foundation (NRF) of Korea under the auspices of the Ministry of Science and ICT, Korea (grant no. NRF-2020R1A2B5B03096000).

Phuong-Tung Pham, Gyoung-Hahn Kim, and Keum-Shik Hong are with the School of Mechanical Engineering, Pusan National University, Busan 46241, Korea (e-mails: {pptung, hahn, kshong}@pusan.ac.kr). Quoc Chi Nguyen is with the Department of Mechatronics, Ho Chi Minh City University of Technology (HCMUT)-Vietnam National University Ho Chi Minh City, 268 Ly Thuong Kiet Street, District 10, Ho Chi Minh City, Vietnam (e-mail: nqchi@hcmut.edu.vn).
* Corresponding author.

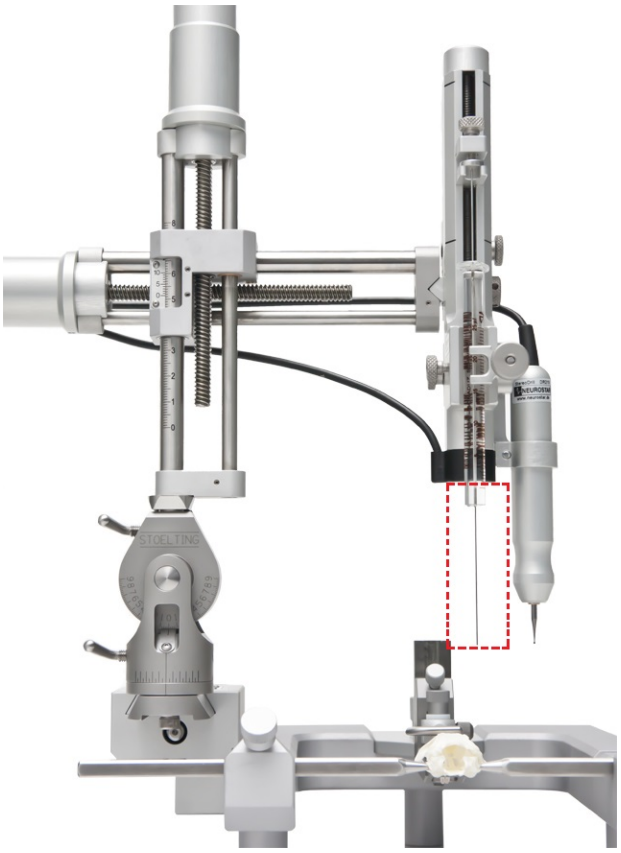

Fig. 1. Drill and microinjection robot [1].

model of a beam is a set of ordinary differential equations (ODEs) that are transformed from the PDE model via approximation methods, such as the Galerkin decomposition method [19,20] and finite element method [11].

In many practical systems, the measurement of system parameters, such as Young's modulus and damping coefficient, are often accompanied by challenges from both technical and economic perspectives. Such challenges lead to difficulty in determining the exact values of the modal parameters. In this situation, experimental identification is regarded as a practical solution for estimating the modal parameters of the vibratory system. Wei *et al.* [21] presented an experimental identification of the natural frequency and damping ratio of a stationary beam, while Liu and Sun [22] and Xie *et al.* [18] published studies on the modal parameter identification of rotating beams. Concerning translating beams, Yang *et al.* [23] investigated the vibrations of a machine tool modeled as a translating beam, wherein the particle swarm optimization algorithm was employed to obtain the beam's modal parameters.

Oscillation suppression of vibratory systems can be performed through either closed-loop or open-loop control [24–35,38]. Closed-loop control approaches generate the control forces/torques based on the feedback signal measured by sensors [32–34], whereas open-loop control laws are designed based on modal parameters. When suppressing a beam's vibration (Fig. 2), input shaping control is known as the most feasible and practical open-loop control technique [35,36]. This technique designs an appropriate command signal that can guarantee the beam's movement to the desired position resulting in minimum residual vibration. Input shaping control has various types, including the zero-vibration (ZV) shaper, zero-vibration derivative (ZVD) shaper, and zero-vibration derivative-derivative (ZVDD) shaper [37], and each of these has its advantages and disadvantages. Input shaping control has been implemented in many vibration problems, including spacecraft, micro-electrical structures, robotics, and cranes [14,38].

To date, experimental studies on input shaping control of a non-uniform beam system based on model parameters have been limited. In this paper, the types of input shaping control for a non-uniform flexible cantilever beam with a translating base (Fig. 2) are investigated. A mathematical model consisting of both beam and base dynamics is first established using the extended Hamilton principle. For convenience in analyzing the modal parameter, an approximate model is developed based on the Galerkin decomposition method. Subsequently, the modal parameters are identified based on the experimental modal analysis (EMA) method. According to these modal parameters, various input shaping controls are designed for two control objectives: i) Moving the beam and base to a desired position and ii) minimizing the beam's residual vibration. The experimental control performances of each type are verified and compared. Accordingly, the advantages and disadvantages of each type are presented and discussed.

The remainder of this paper is organized as follows: Section 2 presents the dynamic model of the non-uniform beam attached to a moving base, including the PDE and ODE models. The procedure for modal parameter identification is introduced in Section 3. The input shaping control design is described in Section 4. In Section 5, the experimental results are presented. Finally, Section 6 concludes the paper.

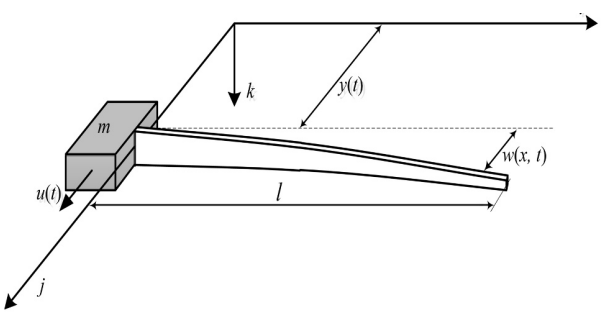

Fig. 2. Example of a non-uniform flexible link clamped into a translating base.

2. DYNAMIC MODEL

Fig. 2 shows a schematic diagram of a beam-base system, where a non-uniform beam of length l is clamped to a base moving along the j-axis. A control force $u(t)$ is applied to the base, and the position of the base is denoted by $y(t)$. The deflection of the beam $w(x, t)$, a spatiotemporal function of x and t, results from the base's motion. Based on the Euler–Bernoulli beam theory, the kinetic energy K, the potential energy P, and the work done W of the system are respectively given as follows:

$$K = \frac{1}{2}m\dot{y}^2(t) + \frac{1}{2}\rho\int_0^l A(x)\left(\dot{y}(t) + w_t(x,t)\right)^2 dx, \quad (1)$$

$$P = \frac{1}{2}E\int_0^l I(x)w_{xx}^2(x,t)dx, \quad (2)$$

$$\delta W = u(t)\delta y, \quad (3)$$

where m is the base's mass, ρ denotes the mass density, E indicates Young's modulus, and $A(x)$ and $I(x)$ are spatial functions corresponding to the cross-sectional area and inertial moment of the beam, respectively. In this study, the subscripts in w_x and w_t are the partial derivatives of the spatiotemporal function $w(x, t)$ with respect to x and t, respectively, whereas $\dot{y}$ (i.e., dy/dt) denotes the total derivative with respect to t. The equations of motion of the system are obtained using Hamilton's principle, i.e.,

$$\rho A(x)\left[\ddot{y}(t) + w_{tt}(x,t)\right] + E\left[I(x)w_{xx}(x,t)\right]_{xx} = 0, \quad (4)$$

$$m\ddot{y}(t) + \rho\int_0^l A(x)\left[\ddot{y}(t) + w_{tt}(x,t)\right]dx = u(t), \quad (5)$$

with the initial and boundary conditions

$$y(0) = \dot{y}(0) = 0, \;\; w(x,0) = w_t(x,0) = 0, \quad (6)$$

$$w(0,t) = w_x(0,t) = 0, \quad (7)$$

$$w_{xx}(l,t) = w_{xxx}(l,t) = 0. \quad (8)$$

Equations (4)-(8) represent the PDE model describing the system's dynamics, where (4) and (5) are the equations of motion of the beam and the base, respectively. Note that the beam dynamics (i.e., (4)) are affected by the base's acceleration, whereas the vibrations of the beam also influence the base's dynamic behaviors (i.e., (5)).

For convenience, using the conventional approach to identify the modal parameters, the PDE model represented by (4)-(8) are approximated as a set of ODEs using the Galerkin method. Accordingly, the transverse displacement of the beam can be represented by

$$w(x,t) = \sum_{i=1}^{n} q_i(t)\varphi_i(x), \quad (9)$$

where $q_i(t)$ is the time-varying variable, and $\varphi_i(x)$ is the basis function expressed as follows [39]:

$$\varphi_i(x) = \frac{1+\cos\lambda_i l\cosh\lambda_i l}{\sin\lambda_i l\sinh\lambda_i l}(2-\cos\lambda_i x-\cosh\lambda_i x) - \frac{\cos\lambda_i l\sinh\lambda_i l+\sin\lambda_i l\cosh\lambda_i l}{\sin\lambda_i l\sinh\lambda_i l} \times (\sin\lambda_i x-\sinh\lambda_i x) + (\cos\lambda_i x-\cosh\lambda_i x), \quad (10)$$

where λ_i is the i-th solution obtained from the frequency equation [40]:

$$1+\cosh(\lambda_i l)\cos(\lambda_i l) + \frac{m_b}{m\lambda_i}\left(\sin(\lambda_i l)\cosh(\lambda_i l)+\cos(\lambda_i l)\sin(\lambda_i l)\right) = 0, \quad (11)$$

where m_b is the mass of the beam. The equation of motion of the beam (4) can be transformed into a set of ODEs by i) substituting (9) into (4), ii) multiplying this equation by the weighting function $\varphi_j(x)$, which has the same form as the basis function, and then iii) integrating the resulting equation over the interval $x \in [0, l]$. Consequently, a set of n ODEs is obtained. By combining this set of ODEs with the equation of motion of the base (i.e., considering (5) as an ODE), we derive the following (n+1)-degree-of-freedom model:

$$\mathbf{M}\ddot{\mathbf{q}} + \mathbf{K}\mathbf{q} = \mathbf{u}, \quad (12)$$

where

$$\mathbf{M} = \begin{bmatrix} J & h_1 & h_2 & \cdots & h_n \\ h_1 & m_{11} & m_{21} & \cdots & m_{n1} \\ h_2 & m_{12} & m_{22} & \cdots & m_{n2} \\ \vdots & \vdots & \vdots & \ddots & \vdots \\ h_n & m_{1n} & m_{2n} & \cdots & m_{nn} \end{bmatrix}, \quad (13)$$

$$\mathbf{K} = \begin{bmatrix} 0 & 0 & 0 & \cdots & 0 \\ 0 & k_{11} & k_{21} & \cdots & k_{n1} \\ 0 & k_{12} & k_{22} & \cdots & k_{nn} \\ \vdots & \vdots & \vdots & \ddots & \vdots \\ 0 & k_{1n} & k_{2n} & \cdots & k_{nn} \end{bmatrix}, \quad (14)$$

$$\mathbf{q} = \begin{bmatrix} y & q_1 & q_2 & \ldots & q_n \end{bmatrix}^{\mathrm{T}}, \quad (15)$$

$$\mathbf{u} = \begin{bmatrix} u & 0 & 0 & \ldots & 0 \end{bmatrix}^{\mathrm{T}}. \quad (16)$$

The elements of the matrices in (13)-(14) are defined as follows:

$$J = m + \rho\int_0^l A(x)dx, \quad (17)$$

$$h_i = \rho\int_0^l A(x)\varphi_i(x)dx, \quad (18)$$

$$m_{ij} = \rho\int_0^l A(x)\varphi_i(x)\varphi_j(x)dx, \quad (19)$$

$$k_{ij} = E\int_0^l \left\{ \varphi_j(x)\frac{d^2}{dx^2}\left(I(x)\frac{d^2\varphi_i(x)}{dx^2}\right)\right\} dx. \tag{20}$$

Equation (12) describes the dynamics of the undamped system. In practical systems, the damping coefficient is very small; therefore, this model is acceptable in many situations. However, because we aim to analyze the modal parameters, such as the natural frequency and damping ratio, it is necessary to include the damping term in (12). We consider the use of classical Rayleigh damping, which is proportional to a linear combination of the system's mass and stiffness. This results in the following damping matrix being added to (12):

$$\mathbf{C} = \alpha_1\mathbf{M} + \alpha_2\mathbf{K}, \tag{21}$$

where α_1 and α_1 are two Rayleigh damping coefficients. These coefficients can be determined via the natural frequency and damping ratio of the vibration modes using the following equation:

$$\zeta_r = \frac{1}{2}\left(\frac{\alpha_1}{\omega_r} + \alpha_2\omega_r\right), \tag{22}$$

where ω_r and ζ_r denote the natural frequency in rad/s and damping ratio of the r-th mode, respectively. Under Rayleigh damping, the damped model of the system is given as follows:

$$\mathbf{M}\ddot{\mathbf{q}} + \mathbf{C}\dot{\mathbf{q}} + \mathbf{K}\mathbf{q} = \mathbf{u}. \tag{23}$$

3. MODAL PARAMETER IDENTIFICATION

Modal parameters, including the natural frequency, damping ratio, and mode shape, indicate the mechanical properties of the vibratory system. Identifying these modal parameters has critical implications for the dynamic analysis and design of an open-loop controller. In this section, the process of modal parameter identification using the EMA approach is discussed.

3.1. Experimental modal analysis

EMA determines the model parameters (i.e., natural frequency, damping ratio, and mode shape) based on experimental data [41,42]. This approach records the excitation force signals and corresponding displacements of the beam in the time domain. Frequency response functions (FRFs), which describe the dynamic behaviors, are then estimated through digital signal processing. Finally, according to these FRFs, the natural frequency and damping ratio can be identified using fitting algorithms, such as the least-squares complex exponential method and peak picking method.

EMA is based on the mode-superposition principle for the ODE model of the beam [43]. For (12), if we consider the free-vibration case, the characteristic equation of the undamped system is given by

$$\det\left(\mathbf{K} - \omega^2\mathbf{M}\right) = 0, \tag{24}$$

where the roots, ${\omega_r}^2$, are the eigenvalues (or squared natural frequencies). The eigenvector corresponding to the r-th eigenvalue ${\omega_r}^2$ is called the r-th mode shape. It is noted that the mode shape of the r-th mode is a vector that can be scaled to have a unique amplitude by nomalization. The resulting vector is called the modal vector of the r-th mode of the undamped system $\mathbf{\Phi}_r$ [43]. Now, we consider the ODE model with N degrees of freedom under a harmonic excitation force as follows:

$$\mathbf{M}\ddot{\mathbf{q}} + \mathbf{C}\dot{\mathbf{q}} + \mathbf{K}\mathbf{q} = \mathbf{u}e^{i\omega_e t}. \tag{25}$$

The model-superposition solution for the steady-state response is derived by

$$\mathbf{q}(t) = \sum_{r=1}^{N} \frac{\mathbf{\Phi}_r\mathbf{\Phi}_r^{\mathrm{T}}\mathbf{u}}{K_r} \frac{1}{\left[1-\left(\frac{\omega_e}{\omega_r}\right)^2\right] + i2\zeta_r\frac{\omega_e}{\omega_r}} e^{i\omega_e t}, \tag{26}$$

where i represents the imaginary unit, ω_e is the excitation frequency in rad/s, ω_r and ζ_r are the natural frequency and damping ratio of the r-th mode, respectively, and $K_r = \mathbf{\Phi}_r^{\mathrm{T}}\mathbf{K}\mathbf{\Phi}_r$ is the modal stiffness of the r-th mode. The frequency-response function at coordinate m due to the harmonic excitation at coordinate n is denoted by H_{mn}. If the response signal is the displacement, it is called the receptance FRF and is defined as the ratio of the displacement signal to the excitation force signal, i.e.,

$$H_{mn}(\omega_e) = \sum_{r=1}^{N} \frac{\phi_{rm}\phi_{rn}}{K_r} \frac{1}{(1-R_r^2) + i(2\zeta_r R_r)}, \tag{27}$$

where $R_r = \omega_e/\omega_r$ is the frequency ratio of the r-th mode, ϕ_{rm} and ϕ_{rn} are the m-th and n-th elements of $\mathbf{\Phi}_r$, respectively. It can be observed that the elements of the FRF matrix are characterized by the natural frequency, damping ratio, and further mode shape of the r-th mode. Therefore, these modal parameters can be estimated by determining and analyzing the FRFs.

The process of the EMA used for identifying the modal parameters can be summarized as follows:

Step 1: Collect the experimental data consisting of the time histories of the excitation force and corresponding displacements of the beam.

Step 2: Estimate the FRFs based on the experimental data and computing power spectral density using the discrete Fourier transform with a Hamming window [44].

Step 3: Identify the natural frequencies and damping ratio corresponding to each natural frequency using the fitting algorithms.

Note that this approach can also identify the mode shape. However, we only need the natural frequencies and damping ratios to design the input shaping control.

3.2. Logarithmic decrement algorithm

Another approach used to determine the damping ratio of underdamped systems is the logarithmic decrement algorithm [45]. This algorithm considers the system as a single-degree-of-freedom harmonic oscillator and derives the damping ratio via successive positive peak amplitudes. Accordingly, the damping ratio can be computed using the following formulation:

$$\zeta = \frac{1}{\sqrt{1+(2\pi/\delta)^2}}, \tag{28}$$

where δ is the logarithmic decrement relating to the natural log of the ratio of the amplitudes of any two successive peaks, i.e.,

$$\delta = \frac{1}{n}\ln\frac{w_1}{w_n}, \tag{29}$$

where w_1 is the first successive peak, and w_n is the amplitude of the n-th successive peak. In this study, the damping ratios of the two first modes are assumed to be equal, and the results evaluated by logarithmic decrement can represent both modes.

4. INPUT SHAPING CONTROL

According to the modal parameters obtained by EMA, an open-loop control scheme is designed based on the input shaping technique for vibration suppression of a beam. The key to this technique is to create an appropriate command signal (i.e., shaped command) to minimize the system's residual vibration. The shaped command is generated by convolving an arbitrary command with a sequence of impulses applied at different times. This sequence of impulses is known as the input shaper. Each impulse of the input shaper is characterized by its amplitude and time location. These values can be determined based on the natural frequency and damping ratio.

The input shaper is designed based on the constraint relating to the percentage vibration (i.e., the percentage vibration is the ratio of the vibration's amplitude for a multi-impulse input and that for a single unity-magnitude impulse). Various input shapers were designed in the literature [37]. The fundamental input shaper, the ZV shaper, is described as follows:

$$\begin{bmatrix} A_1 & A_2 \\ t_1 & t_2 \end{bmatrix} = \begin{bmatrix} \frac{1}{1+K} & \frac{K}{1+K} \\ 0 & \frac{\pi}{\omega\sqrt{1-\zeta^2}} \end{bmatrix}, \tag{30}$$

where $K = e^{-\zeta\pi/\sqrt{1-\zeta^2}}$, and ω is the natural frequency in rad/s. The drawback of the ZV shaper is its high sensitivity to variations in modal parameters. To improve the robustness of the input shaping control, the ZVD and ZVDD shapers can be used. The amplitudes and time locations of the impulses of the ZVD shaper are derived as follows:

$$\begin{bmatrix} A_1 & A_2 & A_3 \\ t_1 & t_2 & t_3 \end{bmatrix} = \begin{bmatrix} \frac{1}{(1+K)^2} & \frac{2K}{(1+K)^2} & \frac{K^2}{(1+K)^2} \\ 0 & \frac{\pi}{\omega\sqrt{1-\zeta^2}} & \frac{2\pi}{\omega\sqrt{1-\zeta^2}} \end{bmatrix}. \tag{31}$$

Those of the ZVDD shaper is derived as follows:

$$\begin{bmatrix} A_1 & A_2 & A_3 & A_4 \\ t_1 & t_2 & t_3 & t_4 \end{bmatrix} = \begin{bmatrix} \frac{1}{(1+K)^3} & \frac{3K}{(1+K)^3} & \frac{3K^2}{(1+K)^3} & \frac{K^3}{(1+K)^3} \\ 0 & \frac{\pi}{\omega\sqrt{1-\zeta^2}} & \frac{2\pi}{\omega\sqrt{1-\zeta^2}} & \frac{3\pi}{\omega\sqrt{1-\zeta^2}} \end{bmatrix}. \tag{32}$$

The input shaping can be extended to a multi-mode system based on the convolution method [46,47]. This is a straightforward method that generates a multi-mode shaper by directly convolving single-mode shapers designed for individual modes. Accordingly, the total number of impulses of a multi-mode shaper is $N = n^m$, where n is the number of impulse of each single-mode shaper, and m is the number of considered modes. In the next section, we report the use of input shaping control to deal with the first two modes of the considered system.

5. EXPERIMENTAL RESULTS

5.1. Experimental system

The experiment aimed to control a stainless steel beam clamped on a moving base. The system parameters were $l = 0.9$ m, $\rho = 8190$ kg·m^{-3}, $E = 190 \times 10^9$ Nm^{-2}, and $m = 2.5$ kg. The testbed shown in Fig. 3 was used to collect the experimental data for EMA and verify the performance of the proposed control laws. The motion of the moving base was controlled by a Yokogawa linear motor using a UMAC motion controller. The motion program controlling the whole linear motor system was generated from the UMAC controller's corresponding software (PeWin32Pro). The beam's vibration was measured by a Keyence high-speed camera with a sampling time of 0.01 s.

5.2. Parameter identification

The modal parameters of the first two modes were identified based on EMA using the input/output experimental data. The input signal was the excitation force, and the output signal was the displacement of the beam's tip. The input/output data in the time domain were collected via a sine sweep test, where the instantaneous frequency of the excitation input was varied with time. Two sweep types, linear sweep and exponential sweep, were considered. The linear and exponential sweep rates, respectively, are defined as follows:

$$\beta_{\text{linear}} = (f_b - f_a)/T, \tag{33}$$

$$\beta_{\text{exp}} = \frac{\ln(f_b/f_a)}{\ln(2)}\frac{60}{T}, \tag{34}$$

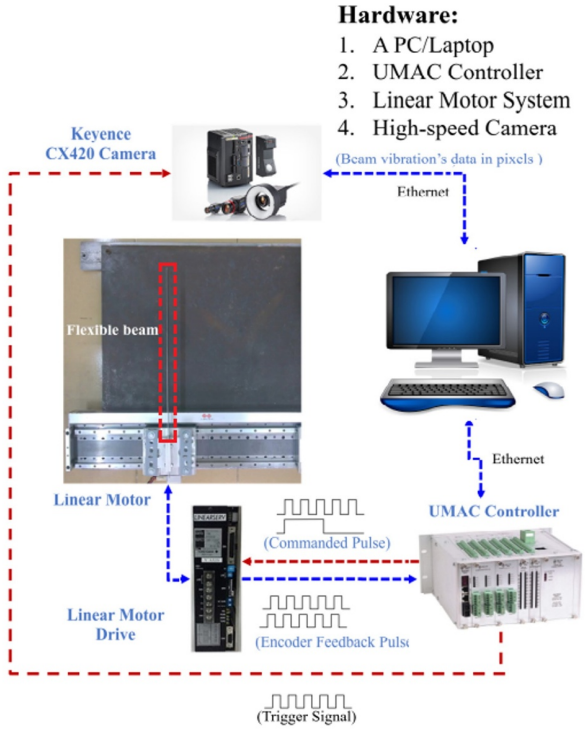

Fig. 3. Experimental testbed [48].

where $f_a = 0.1$ Hz and $f_b = 8$ Hz are the lower and upper frequency limits, respectively, and T is the testing time. The input/output signals in the time domain were recorded by a vision system using the Keyence high-speed camera. Accordingly, the frequency-response functions were determined using the discrete Fourier transform with a Hamming window. The spectra of the system under differential excitations are illustrated in Fig. 4. Based on these FRFs, the modal parameters could be identified using the least-squares complex exponential method. Table 1 lists the estimated modal parameters under various sweep rates. It can be seen that most of the natural frequencies estimated using the exponential sweeps are similar (i.e., the first- and second-mode frequencies are all approximately 1.1 and 6.9 Hz, respectively). The percentage difference between the estimated frequencies did not exceed 0.4%. In contrast, the percentage difference between the damping ratios is considerable at more than 40%. Furthermore, the first natural frequency and first damping ratio estimated based on the linear sweep are significantly different from those in other cases. This is because of the disadvantage of using linear sweep in handling systems, wherein the first natural frequency is close to the lower limit frequency [49].

Besides the damping ratios identified based on EMA, these parameters can be estimated using the logarithmic decrement. In this experiment, the assumption that the damping ratios of the two first modes are equal was ac-

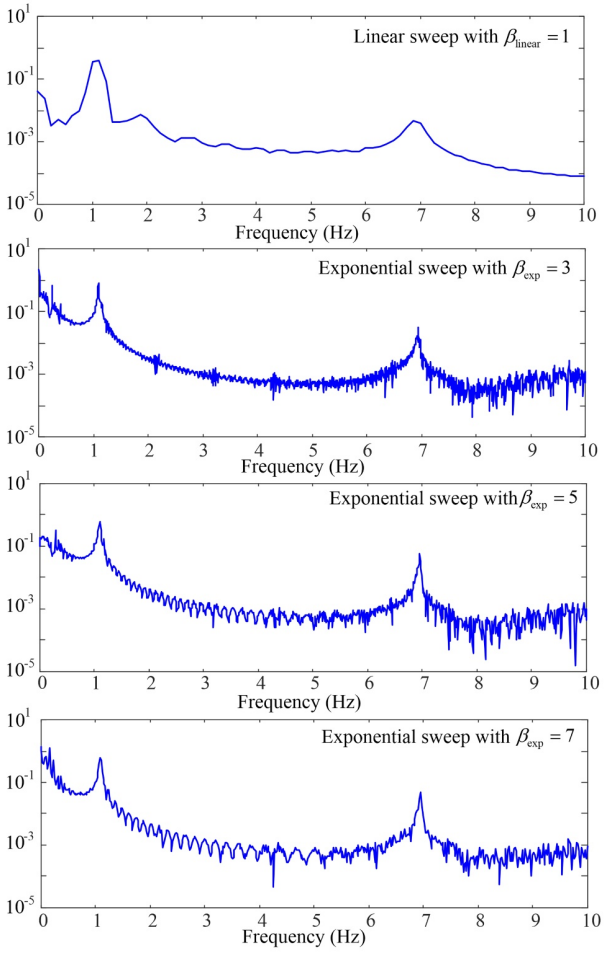

Fig. 4. Spectra of the system under differential excitations.

Table 1. Estimated modal parameters.

Sweep type	Natural frequency		Damping ratio	
	First mode	Second mode	First mode	Second mode
Linear $\beta_{linear} = 1$	1.0063	7.0017	0.0011	0.0089
Exponential $\beta_{exp} = 3$	1.0951	6.8917	0.0071	0.0059
Exponential $\beta_{exp} = -5$	1.0988	6.9146	0.0059	0.0033
Exponential $\beta_{exp} = 7$	1.0976	6.9196	0.0083	0.0012

ceptable. The free vibration response shows that the decaying rate significantly depends on the first mode, and the damping ratio estimated by the logarithmic decrement is close to this mode. Based on the first two successive positive peaks, the following damping ratios are obtained:

$$\zeta_1 = \zeta_2 = 0.0074. \tag{35}$$

There is a considerable difference between the damping

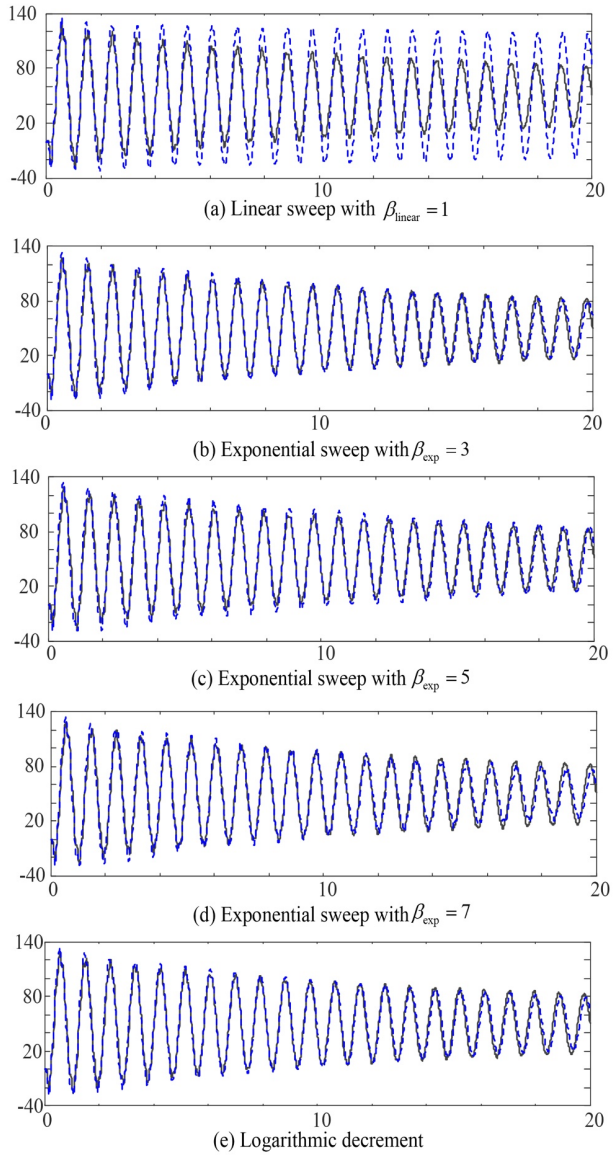

Fig. 5. Comparison between the actual model and estimated ones: The solid and dashed lines indicate the responses of the actual model and the estimated ones with different natural frequencies and damping ratios.

ratios estimated by the different methods. We performed simulation verifications to determine the two damping ratios of the first two modes showing the closest behavior with the experimental data. The Rayleigh damping coefficients for each case are computed based on the natural frequencies and damping ratios of the first two modes. According to these values and (21), the vibration responses for each case could be obtained via simulation. Fig. 5 compares the experimental and simulated vibration results. It can be seen that the damping ratios under the linear sine sweep are too small; hence, the modal parameters of this case cannot be used to describe the system dynamics. On the contrary, the model using the damping ratios under the exponential sine sweep and logarithmic decrement can capture the dynamics of the actual system. Therefore, we can use these damping ratios to design the shaper of the input shaping control. The insignificant error of the estimated modal parameters can be handled by the robustness of the ZVD and ZVDD shapers.

Table 2. Comparison of input shaping controllers.

	Input shaper	Settling time	Overshoot (%)	Percentage vibration (%)
Single-mode	ZV	0.73	22.04	5.83
	ZVD	1.12	14.96	3.62
	ZVDD	1.57	8.48	2.84
Two-mode	ZV	0.75	13.18	1.96
	ZVD	1.27	6.86	1.26
	ZVDD	1.75	2.26	0.36

5.3. Input shaping control

The control objective is to move the base from 0 to 50 mm and minimize the residual vibration of the beam's tip. Furthermore, this study aims to reduce the percentage vibration to below 2%. Because most of the vibration problem is caused by the first flexible mode of the system, we first consider the system under the single-mode input shaping control. The shapers are designed based on the first natural frequency $f_1 = 1.1$ Hz and the damping ratio $\zeta_1 = 0.0074$. Fig. 6 shows the performance of the single-mode ZV shaper. In this case, the percentage vibration is less than 6%. The ZVD and ZVDD shapers slightly improve the input shaping control performances, where residual vibration is reduced to less than 4% and 3%, respectively, compared to the uncontrolled systems (see Fig. 7). Although the performance of the single-mode input shaping control is good, the percentage vibration is still larger than 2%. This is due to influence from the higher modes on the residual vibration. The controller's performance can be further improved by including the shapers for the second mode.

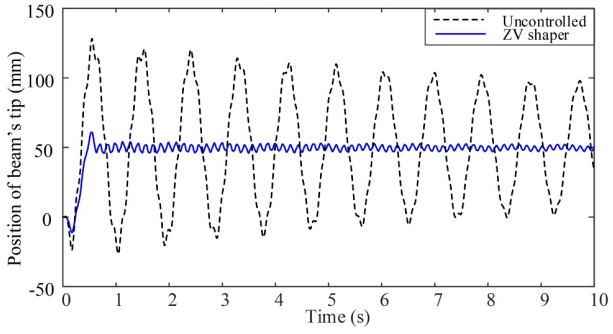

Fig. 6. Single-mode ZV input shaping control.

The responses of the beam's tip under the two-mode ZV shaper and two-mode ZVD and ZVDD shapers are shown in Figs. 8 and 9, respectively. The residual vibration is sharply suppressed, and the goal of 2% percentage vibration is achieved. Table 2 lists the percentage vibration, settling time, and system overshoot results under different input shaping control laws. It can be seen that the two-mode shapers suppress vibration more efficiently than the single-mode shapers. In addition, the residual vibrations of the system using the ZVD and ZVDD shapers are smaller than those using the ZV shaper due to the robustness of these shapers. However, as mentioned in Section 4, the time locations of the final impulses of the ZVD and ZVDD shapers is larger than that of the ZV shaper. This results in a significant difference in the settling time of the system under these shapers. As shown in Table 3, the settling time of the system under the ZVDD shaper is three times that under the ZV shaper. The differences in the settling time between the first mode and convolution of the two modes are small; however, the increments of residual vibrations are considerable, corresponding to at least 50% of the improvement.

6. CONCLUSION

In this study, single- and multi-mode input shaping controls of a non-uniform flexible beam attached to a moving base were investigated. The mathematical model of the beam and base system was developed based on Hamilton's principle. An approximated model with a finite number of vibration modes was also established via the Galerkin method. The experimental modal analysis was conducted to identify the natural frequencies and damping ratios. Both single- and two-mode input shaping controllers with ZV, ZVD, and ZVDD shapers were designed using the estimated modal parameters. The experimental results were used to compare the performances of the single- and two-mode input shaping controllers. Although the settling time of the latter was slightly larger than that of the former, its effectiveness in vibration suppression was improved significantly.

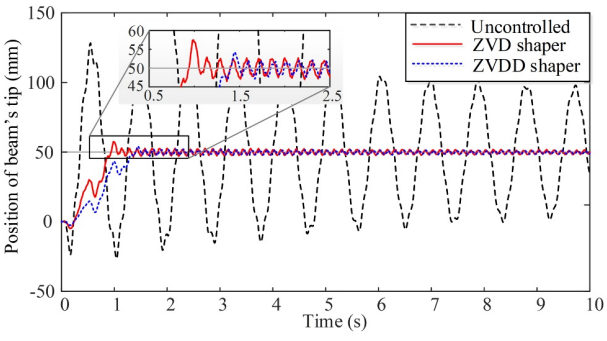

Fig. 7. Single-mode ZVD and ZVDD input shaping control.

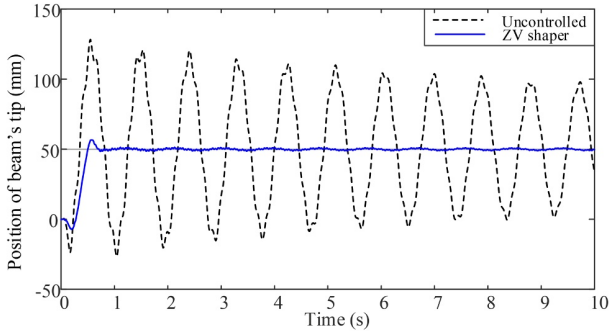

Fig. 8. Two-mode ZV input shaping control.

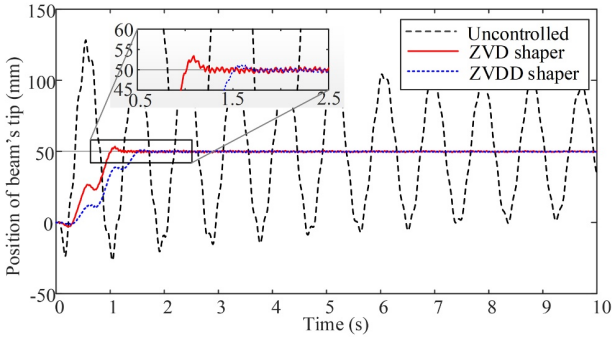

Fig. 9. Two-mode ZVD and ZVDD input shaping control.

REFERENCES

[1] "Drill and Injection Robot," Accessed on Jan. 28, 2021 [Online]. Available: http://nbtltd.com/ products/drill-and-injection-robot/.

[2] M. Dadfarnia, N. Jalili, B. Xian, and D. M. Dawson, "Lyapunov-based vibration control of translational Euler-Bernoulli beams using the stabilizing effect of beam damping mechanisms," *Journal of Vibration and Control*, vol. 10, no. 7, pp. 933-961, 2004.

[3] W. He and S. S. Ge, "Vibration control of a flexible beam with output constraint," *IEEE Transactions on Industrial Electronics*, vol. 62, no. 8, pp. 5023-5030, 2015.

[4] P. Shi, J. McPhee, and G. R. Heppler, "A deformation field for Euler-Bernoulli beams with applications to flexible multibody dynamics," *Multibody System Dynamics*, vol. 5, no. 1, pp. 79-104, 2001.

[5] B. A. H. Abbas, "Dynamic stability of a rotating Timoshenko beam with a flexible root," *Journal of Sound and Vibration*, vol. 108, no. 1, pp. 25-32, 1986.

[6] T. Yokoyama, "Vibrations of a hanging Timoshenko beam under gravity," *Journal of Sound and Vibration*, vol. 141, no. 2, pp. 245-258, 1990.

[7] S. M. Han, H. Benaroya, and T. Wei, "Dynamics of transversely vibrating beams using four engineering theories," *Journal of Sound and Vibration*, vol. 225, no. 5, pp. 935-988, 1999.

[8] P.-T. Pham and K.-S. Hong, "Dynamic models of axially moving systems: A review," *Nonlinear Dynamics*, vol. 100, no. 1, pp. 315-349, 2020.

[9] T. Yokoyama, "Free-vibration characteristics of rotating Timoshenko beams," *International Journal of Mechanical Sciences*, vol. 30, no. 10, pp. 743-755, 1988.

[10] Q. C. Nguyen and K.-S. Hong, "Stabilization of an axially moving web via regulation of axial velocity," *Journal of Sound and Vibration*, vol. 330, no. 20, pp. 4676-4688, 2011.

[11] J. H. Fan, D. G. Zhang, and H. Shen, "Dynamic modeling and simulation of a rotating flexible hub-beam based on different discretization methods of deformation fields," *Archive of Applied Mechanics*, vol. 90, no. 2, pp. 291-304, 2020.

[12] Z. C. Qiu, J. D. Han, X. M. Zhang, Y. C. Wang, and Z. W. Wu, "Active vibration control of a flexible beam using a non-collocated acceleration sensor and piezoelectric patch actuator," *Journal of Sound and Vibration*, vol. 326, no. 3-5, pp. 438-455, 2009.

[13] M. H. Tso, J. Yuan, and W. O. Wong, "Suppression of random vibration in flexible structures using a hybrid vibration absorber," *Journal of Sound and Vibration*, vol. 331, no. 5, pp. 974-986, 2012.

[14] U. H. Shah and K.-S. Hong, "Input shaping control of a nuclear power plant's fuel transport system," *Nonlinear Dynamics*, vol. 77, no. 4, pp. 1737-1748, 2014.

[15] H. H. Yoo and S. H. Shin, "Vibration analysis of rotating cantilever beams," *Journal of Sound and Vibration*, vol. 212, no. 5, pp. 807-828, 1998.

[16] J. S. Fang, D. Zhou, and Y. Dong, "Three-dimensional vibration of rotating functionally graded beams," *Journal of Vibration and Control*, vol. 24, no. 15, pp. 3292-3306, 2018.

[17] T. R. Kane, R. R. Ryan, and A. K. Banerjee, "Dynamics of a cantilever beam attached to a moving base," *Journal of Guidance Control and Dynamics*, vol. 10, no. 2, pp. 139-151, 1987.

[18] Y. Xie, P. Liu, and G. P. Cai, "Frequency identification of flexible hub-beam system using control data," *International Journal of Acoustics and Vibration*, vol. 21, no. 3, pp. 257-265, 2016.

[19] K. M. Liew, H. K. Lim, M. J. Tan, and X. Q. He, "Analysis of laminated composite beams and plates with piezoelectric patches using the element-free Galerkin method," *Computational Mechanics*, vol. 29, no. 6, pp. 486-497, 2002.

[20] M. C. Amirani, S. M. R. Khalili, and N. Nemati, "Free vibration analysis of sandwich beam with FG core using the element free Galerkin method," *Composite Structures*, vol. 90, no. 3, pp. 373-379, 2009.

[21] S. Wei, S. Q. Chen, Z. K. Peng, X. J. Dong, and W. M. Zhang, "Modal identification of multi-degree-of-freedom structures based on intrinsic chirp component decomposition method," *Applied Mathematics and Mechanics-English Edition*, vol. 40, no. 12, pp. 1741-1758, 2019.

[22] K. Liu and X. Sun, "System identification and model reduction for a single-link flexible manipulator," *Journal of Sound and Vibration*, vol. 242, no. 5, pp. 867-891, 2001.

[23] M. X. Yang, Y. Dai, Q. Huang, X. Mao, L. Li, X. Jiang, and Y. Peng, "A modal parameter identification method of machine tools based on particle swarm optimization," *Proceedings of the Institution of Mechanical Engineers Part C-Journal of Mechanical Engineering Science*, vol. 233, no. 17, pp. 6112-6123, 2019.

[24] R. F. Fung, Y. T. Liu, and C. C. Wang, "Dynamic model of an electromagnetic actuator for vibration control of a cantilever beam with a tip mass," *Journal of Sound and Vibration*, vol. 288, no. 4-5, pp. 957-980, 2005.

[25] S. M. Khot, N. P. Yelve, R. Tomar, S. Desai, and S. Vittal, "Active vibration control of cantilever beam by using PID based output feedback controller," *Journal of Vibration and Control*, vol. 18, no. 3, pp. 366-372, 2012.

[26] K.-S. Hong and P.-T. Pham, "Control of axially moving systems: A Review," *International Journal of Control Automation and Systems*, vol. 17, no. 12, pp. 2983-3008, 2019.

[27] M. A. Eshag, L. Ma, Y. K. Sun, and K. Zhang, "Robust boundary vibration control of uncertain flexible robot manipulator with spatiotemporally-varying disturbance and boundary disturbance," *International Journal of Control Automation and Systems*, vol. 19, no. 2, pp. 788-798, 2021.

[28] G. H. Kim, P.-T. Pham, Q. H. Ngo, and Q. C. Nguyen, "Neural network-based robust anti-sway control of an industrial crane subjected to hoisting dynamics and uncertain hydrodynamic forces," *International Journal of Control Automation and Systems*, vol. 19, pp. 1953-1961, 2021.

[29] Q. C. Nguyen and K.-S. Hong, "Asymptotic stabilization of a nonlinear axially moving string by adaptive boundary control," *Journal of Sound and Vibration*, vol. 329, no. 22, pp. 4588-4603, 2010.

[30] Q. C. Nguyen and K.-S. Hong, "Simultaneous control of longitudinal and transverse vibrations of an axially moving string with velocity tracking," *Journal of Sound and Vibration*, vol. 331, no. 13, pp. 3006-3019, 2012.

[31] Q. C. Nguyen, M. Piao, and K.-S. Hong, "Multivariable adaptive control of the rewinding process of a roll-to-roll system governed by hyperbolic partial differential equations," *International Journal of Control Automation and Systems*, vol. 16, no. 5, pp. 2177-2186, 2018.

[32] W. He, T. Wang, X. He, L. J. Yang, and O. Kaynak, "Dynamical modeling and boundary vibration control of a rigid-flexible wing system," *IEEE/ASME Transactions on Mechatronics*, vol. 25, no. 6, pp. 2711-2721, 2020.

[33] W. He, T. Meng, X. He, and C. Sun, "Iterative learning control for a flapping wing micro aerial vehicle under distributed disturbances," *IEEE Transactions on Cybernetics*, vol. 49, no. 4, pp. 1524-1535, 2018.

[34] W. He, H. Gao, C. Zhou, C. Yang, and Z. Li, "Reinforcement learning control of a flexible two-link manipulator: An experimental investigation," to appear in *IEEE Transactions on Systems, Man, and Cybernetics: Systems*, Mar. 2020. DOI: 10.1109/TSME.2020.2975232

[35] C. G. Kang, R. Hassan, and K. Y. Kim, "Analysis of a generalized ZVD shaper using impulse vectors," *International Journal of Control Automation and Systems*, vol. 18, no. 8, pp. 2088-2094, 2020.

[36] T. Zhang, M. H. Zhang, and Y. B. Zou, "Time-optimal and smooth trajectory planning for robot manipulators," *International Journal of Control Automation and Systems*, vol. 19, no 1, pp. 512-531, 2021.

[37] W. Singhose, "Command shaping for flexible systems: A review of the first 50 years," *International Journal of Precision Engineering and Manufacturing*, vol. 10, no. 4, pp. 153-168, 2009.

[38] K.-S. Hong and U. H. Shah, *Dynamics and Control of Industrial Cranes*, Springer, Singapore, 2019.

[39] U. H. Shah, K.-S. Hong, and S.-H. Choi, "Open-loop vibration control of an underwater system: application to refueling machine," *IEEE/ASME Transactions on Mechatronics*, vol. 22, no. 4, pp. 1622-1632, 2017.

[40] S. Park, W. K. Chung, Y. Youm, and J. W. Lee, "Natural frequencies and open-loop responses of an elastic beam fixed on a moving cart and carrying an intermediate lumped mass," *Journal of Sound and Vibration*, vol. 230, no. 3, pp. 591-615, 2000.

[41] N. M. M. Maia and J. M. M. Silva, *Theoretical and Experimental Modal Analysis*, Wiley, New York, 1997.

[42] R. Craig and A. Kurdila, *Fundamentals of Structural Dynamics*, John Wiley & Sons. Inc, New Jersey, 2006.

[43] J. D. Ewins, *Model Testing: Theory, Practice and Application*, Research Studies Press, Hertfordshire, 2006.

[44] A. Brandt, *Noise and Vibration Analysis: Signal Analysis and Experimental Procedures*, John Wiley & Sons, Chichester, 2011.

[45] D. J. Inman, *Engineering Vibration*, Pearson Education, Inc., New Jersey, 2008.

[46] N. C. Singer, *Residual Vibration Reduction in Computer Controlled Machines*, Massachusetts Institute of Technology, Cambridge, 1989.

[47] N. C. Singer and W. P. Seering, "Preshaping command inputs to reduce system vibration," *Journal of Dynamic Systems Measurement and Control-Transactions of the ASME*, vol. 112, no. 1, pp. 76-82, 1990.

[48] N. T. G. Vu, *Control of a 3D Flexible Cantilever Beam*, M.S. thesis, Dept. of Mechatronics, Ho Chi Minh City Univ. of Tech., Ho Chi Minh City, 2020.

[49] N. Roy, M. Violin, and E. Cavro, "Sine sweep effect on specimen modal parameters characterization," *Advances in Aircraft and Spacecraft Science*, vol. 5, no. 2, pp. 187-204, 2018.

Phuong-Tung Pham received his B.S. and M.S. degrees in mechanical engineering from Ho Chi Minh City University of Technology, in 2016 and 2018, respectively. He is currently a Ph.D. candidate in the School of Mechanical Engineering, Pusan National University, Korea. His research interests include nonlinear control, adaptive control, vibration control, and control of distributed parameter systems.

Gyoung-Hahn Kim received his B.S. degree in mechanical engineering from Yeungnam University, Gyeongsan, in 2013 and his Ph.D. degree in mechanical engineering, Pusan National University, Busan, Korea, in 2021. He is currently a Postdoctoral Fellow in the Institute of Intelligent Logistics and Big Data, Pusan National University. Dr. Kim's current research interests include sliding mode control, adaptive neural network control, reinforcement deep learning, nonlinear system identification, data-driven control, and control applications to industrial robotics.

Quoc Chi Nguyen received his B.S. degree in mechanical engineering from Ho Chi Minh City University of Technology (HCMUT), Vietnam, in 2002, an M.S. degree in cybernetics from HCMUT, Vietnam, in 2006, and a Ph.D. degree in mechanical engineering from the Pusan National University, Korea, in 2012. Dr. Nguyen was a Marie Curie FP7 postdoctoral fellow at the School of Mechanical Engineering, Tel Aviv University, from 2013 to 2014. He is currently an associate professor with the Department of Mechatronics, HCMUT. Dr. Nguyen's current research interests include nonlinear systems theory, adaptive control, robotics, and distributed parameter systems.

Keum-Shik Hong Please see vol. 17, no. 12, p. 3008, December, 2019 of this journal.